Journal of Tropical Biodiversity and Biotechnology
Volume 11, Issue 01 (2026): jtbb20259
DOI: 10.22146/jtbb.20259

Research Article

Metabolic Adaptation of *Chlorella vulgaris* InaCCM49 to Cadmium-Salinity Stress: UPLC-MS/MS-Based Identification of Antioxidant Metabolites

Dini Ermavitalini[1,2]*, Ratna Syifa'a Rahmahana[1], Anisa Esti Rahayu[3], Hery Purnobasuki[4], Ni'matuzahroh[4]

1)Department of Biology, Faculty of Science and Data Analytics, Sepuluh Nopember Institute of Technology. ITS Campus Keputih Sukolilo Surabaya 6011, East Java, Indonesia
2)Doctoral Study Program of Mathematics and Natural Science, Faculty of Science and Technology, Airlangga University, Jl. Dr. Ir. H. Soekarno, Mulyorejo, Surabaya 60115, East Java, Indonesia
3)Occupational Safety and Health Engineering Study Program, Shipbuilding Institute of Polytechnic Surabaya (PPNS), Jl. Teknik Kimia, Kampus ITS, Sukolilo, Surabaya 60111, East Java, Indonesia
4)Department of Biology, Faculty of Science and Technology, Airlangga University, Jl. Dr. Ir. H. Soekarno, Mulyorejo, Surabaya 60115, East Java, Indonesia
* Corresponding author, email: dini_ermavitalini@its.ac.id

Keywords:
Antioxidant activity
Cadmium stress
Chlorella vulgaris InaCCM49
Untargeted metabolomics
Salinity stress
Submitted:
10 March 2025
Accepted:
20 August 2025
Published:
20 February 2026
Editors:
Furzani Binti Pa'ee
Sri Nopitasari

ABSTRACT

Chlorella vulgaris is a microalga species studied for its characteristics and potential applications since 1960. This study investigates the effect of combined salinity and cadmium stress on compound diversity, antioxidant activity, and pigment concentrations in *C. vulgaris* InaCCM49. Microalgae were cultivated in control and Cd-saline treatments (0.4 M NaCl and 95 µM $CdCl_2$), followed by biomass harvesting, pigment determination, IC_{50} measurement, and metabolomic analysis. Cd-salinity stress enhanced antioxidant activity, showing 51.8% lower IC_{50} values (79.47 ppm) compared to controls (164.99 ppm), and increased carotenoid content to 1.919 mg g^{-1}. Meanwhile, chlorophyll a and b concentrations were notably higher in control treatment during the half-logarithmic phase. Partial Least Squares Discriminant Analysis revealed clear metabolomic differences between treatments. Stigmatellin Y, maltose, glycolipid 1-hexadecanoyl-3-(6'-sulfo-α-D-quinovosyl)-sn-glycerol, and phenolic derivative (2-phenoxy-3-pyridinyl)[3-(2-thienyl)-1H-pyrazol-1-yl] methanone exhibited VIP scores >15. Stigmatellin Y and glycolipids were highly synthesized in controls, whereas maltose and phenolic derivatives were elevated in Cd-saline treatment. Pheophorbide a and 3-oxo-nonadecanoic acid showed the strongest negative correlations with IC_{50} (regression coefficients of -14.6047 and -13.9555), indicating key roles in antioxidant activity. This study represents the first comprehensive metabolomic analysis of *C. vulgaris* InaCCM49 under combined cadmium-salinity stress, revealing metabolic adaptation through enhanced synthesis of phenolic derivatives and pheophorbide a-mediated antioxidant responses.

How to cite:
Ermavitalini, D. et al., 2026. Metabolic Adaptation of *Chlorella vulgaris* InaCCM49 to Cadmium-Salinity Stress: UPLC-MS/MS-Based Identification of Antioxidant Metabolites. *Journal of Tropical Biodiversity and Biotechnology*, 11(1), jtbb20259. doi: 10.22146/jtbb.20259

INTRODUCTION

Microalgae have been explored for commercial applications since the 1960s, with increasing interest due to their potential as sources of primary and secondary metabolites. Among these, *Chlorella vulgaris* is widely studied for its applications in biofuel production, bioremediation, cosmeceuticals, and as a nutritional supplement, owing to its rich composition of bioactive compounds including phenolic, flavonoids, and carotenoids, which contribute to its significant antioxidant capacity as measured by ABTS radical scavenging activity (Pantami et al. 2020; Coronado-Reyes et al. 2022). The ability of *C. vulgaris* to produce a variety of metabolites under different conditions makes it an excellent model organism for studying metabolic adaptations and bioactive compound synthesis. However, the biotechnological potential of microalgae is significantly influenced by environmental challenges that can either enhance or compromise their metabolic performance.

Environmental stress plays a crucial role in modulating the biosynthesis of protective metabolites, including antioxidants, in *C. vulgaris*. Several studies have demonstrated that abiotic stressors influence secondary metabolism by altering cellular defence mechanisms and triggering adaptive responses that affect overall metabolite production and antioxidant capacity (Elfayoumy et al. 2021; Hiremath & Mathad 2022; Wang et al. 2022; Zhang et al. 2023). Zhang et al. (2023) showed that UV-B and salt stress elevated phenolic and flavonoid levels in *C. vulgaris*, enhancing antioxidant enzyme activities, while Wang et al. (2022) found that nitrogen deprivation and salinity stress synergistically increased carotenoid and lipid antioxidant content, supporting the notion that combined abiotic stresses can substantially boost secondary metabolite production.

Among various abiotic stressors, the combination of heavy metal contamination and salinity presents a particularly complex challenge in coastal and industrial environments. Heavy metal exposure, particularly cadmium (Cd), has been reported to induce oxidative stress, which triggers metabolic adjustments affecting photosynthetic pigments, lipid metabolism, and antioxidant responses (Xu et al. 2024). Chlorophyll biosynthesis and degradation are significantly altered under Cd stress, leading to modifications in photosynthetic efficiency (Atabayeva et al. 2022). Similarly, carotenoid biosynthesis is upregulated as a defence mechanism against oxidative damage, while lipid metabolism undergoes substantial modifications with changes in key membrane lipids such as acetone mobile polar lipids (AMPL) and phospholipids (PL), accompanied by accumulation of stress-responsive fatty acids and lipid derivatives (Chia et al. 2013; Shi et al. 2020). The synergistic effects of combined Cd-salinity stress on metabolomic profiles remain largely unexplored despite their environmental relevance.

While individual effects of Cd or salinity stress on *C. vulgaris* metabolism have been studied, comprehensive metabolomic analysis of combined stress responses remain limited. Furthermore, strain-specific responses have received insufficient attention in metabolomics research. Unlike the Indonesian strain InaCCM49, strain UTEX 395 has been extensively characterised using a genome-scale metabolic model (iCZ843), demonstrating strong adaptability across trophic modes through upregulated amino acid, pigment, and lipid biosynthesis under nutrient stress. In contrast, CCAP 211/11B (equivalent to SAG 211-11B) exhibits high halotolerance, sustaining growth and lipid accumulation in seawater, indicating greater salinity resilience compared to UTEX 395. Given the complexity of metabolic changes induced by stress, untargeted metabolomics approaches, particularly chemometric techniques such as Partial Least Squares (PLS) regression, are effective for establishing correlations between metabolite profiles and biological activities, enabling identification of key metabolites contributing to stress tolerance and

antioxidant capacity (Hawrył et al. 2020; Umar et al. 2021).

This study focuses on investigating the effect of combined salinity and cadmium stress on compound diversity, antioxidant activity, chlorophyll, and carotenoid pigment concentrations in *C. vulgaris* InaCCM49, while evaluating compounds contributing to IC_{50} values through UPLC-MS/MS and PLS analysis. By integrating untargeted metabolomics with multivariate statistical analysis, this research aims to elucidate key metabolic pathways underlying the dual stress response and identify bioactive compounds contributing to antioxidant potential. Understanding the metabolic adaptations of *C. vulgaris* InaCCM49 will provide insights into strain-specific biotechnological applications and the potential for producing bioactive compounds with significant antioxidant properties under environmentally relevant stress conditions.

MATERIALS AND METHODS

Materials

Chlorella vulgaris InaCCM49 was obtained from the Indonesian Culture Collection of Microorganisms (InaCCM), National Research and Innovation Agency (BRIN), Indonesia. The strain was maintained under standard laboratory conditions at pH 7.0 ± 0.2, 25 °C ± 2 °C, with continuous illumination of 50 µmol photons m^{-2} s^{-1} under a 12:12 h light:dark cycle, in BG-11 medium. Baseline measurements for cell density, chlorophyll content, carotenoid levels, and antioxidant activity were established from control cultures prior to stress treatment application.

Equipment and reagents used included: Low Speed Cryogenic Universal Centrifuge (Centrifuge 5430, Eppendorf), Vortex mixer (QL-901, Kylin-Bell Lab Instruments Co., Ltd China), Ultrapure water meter (Milli-Q Integral, Millipore Corporation, USA), Refrigerated Vacuum Concentrator (Maxi Vac-beta, Gene Company), Tissue Grinder (JXFSTPRP, Shanghai Xin Ning, China), Methanol (A454-4), Acetonitrile (A998-4) were all LCMS level (Thermo Fisher Scientific, USA), Ammonia formate (17843-250G, Honeywell Fluka, USA), Formic acid (50144-50 ml, Dimka, USA). Ultrapure water (18.2 MΩ·cm) was generated using a Milli-Q system (Millipore). Internal standards used were: d3-Leucine, 13C9-Phenylalanine, d5-Tryptophan, and 13C3-Progesterone.

Methods

Microalgae cultivation

A total of 20 % (v/v) of 6-day-old *C. vulgaris* InaCCM49 microalgae starter culture was cultivated in vitro in control treatment using artificial seawater media Blue Treasure™ added with sterile Walne nutrients as much as 1 mL L^{-1}. Artificial seawater was prepared using commercial salt (Blue Treasure SPS Sea Salt™, China) dissolved in ultrapure water. The seawater salt mixture at salinity of 35‰ contains: Na^+ = 9300 mg L^{-1}, Cl^- = 17300 mg L^{-1}, Ca^{2+} = 430 mg L^{-1}, Mg^{2+} = 1400 mg L^{-1}, K^+ = 360 mg L^{-1}, SO_4^{2-} = 2260 mg L^{-1}, Sr^{2+} = 9.0 mg L^{-1}, Rb^{2+} = 0.11 mg L^{-1}, Fe = 0.06 mg L^{-1}, Br^- = 20 mg L^{-1}, B = 4.0 mg L^{-1}, F^- = 0.8 mg L^{-1}, and trace elements. Cultivation conditions were of 25 °C, medium pH 7.5-8, continuous 24-hour irradiation, aeration with oxygen bubbling, 2 % of CO2 levels, light intensity of 4000 lux, and salinity of 35 ‰. The nutrient solution was prepared according to Walne (1970) containing per litre: $NaNO_3$ 100.0 g, $NaH_2PO_4{\cdot}2H_2O$ 20.0 g, EDTA (disodium salt) 45.0 g, $FeCl_3{\cdot}6H_2O$ 1.3 g, $MnCl_2{\cdot}4H_2O$ 0.36 g, H_3BO_3 33.6 g, and trace metal solution (TMS) 1.0 mL containing $ZnCl_2$ 2.1 g, $CoCl_2{\cdot}6H_2O$ 2.0 g, $(NH_4)_6Mo_7O_{24}{\cdot}4H_2O$ 0.9 g, and $CuSO_4{\cdot}5H_2O$ 2.0 g per 100 mL. The solution was acidified to clarify concentrated HCl and sterilised by autoclaving at 15 psi for 15 minutes. Unlike Xu et al. (2024), who investigated single cadmium stress on *Scenedesmus obliquus* with concentrations ranging from 0.005–10 mg

L^{-1} (EC_{50} = 0.41 ± 0.03 mg L^{-1} after 96 hours), our study employed a combined stress approach by adding 0.4 M NaCl and 95 µM $CdCl_2$ (approximately 10.7 mg L^{-1}) to the cultivation medium from day 0 to simulate realistic coastal pollution conditions where cadmium contamination co-occurs with salinity stress, representing a supra-lethal dose designed to elicit strong metabolic responses. While Xu et al. (2024) monitored *Scenedesmus obliquus* responses every 24 hours over 96 hours during logarithmic growth phase, our extended sampling protocol captured metabolic dynamics across different growth phases based on preliminary IC_{50} experiments at three critical timepoints: mid-exponential phase (5 days), late-exponential phase (8 days), and death phase (12 days). Metabolomic samples were collected in triplicate during the highest IC_{50} phase (day 5) to capture peak metabolic stress responses when cellular adaptation mechanisms are most active. Microalgal growth under control and stress treatments was measured by calculating cell density using a Neubauer's chamber Haemocytometer, weighing dry biomass, and measuring optical density (OD) with a UV-Vis spectrophotometer at λ 680 nm every 24 hours until reaching the death phase (Gonzalez-Esquer et al. 2019).

Microalgae harvesting

The harvesting of microalgae in stress and control treatments was performed at three different growth phases, namely at half-logarithmic phase, end of logarithmic phase, and death phase. Phase selection was based on established protocols for capturing stress-adaptive metabolites across different physiological states, as metabolite profiles vary significantly during algal growth cycles under abiotic stress conditions (Gonzalez-Esquer et al. 2019). The half-logarithmic phase represents active cell division with high metabolic activity; the end logarithmic phase indicates nutrient limitation onset, and the death phase reflects maximum stress response, collectively providing comprehensive metabolomic insights into *C. vulgaris* adaptation mechanisms (Chen et al. 2020; Liu et al. 2021). Microalgae were separated from the medium by centrifugation technique at a speed of 3000 rpm for 10 minutes. A total of 1-10 mg of filtered biomass was then diluted with 25 mL of 0.5 M ammonium formate to remove salt residues from the cell culture. Furthermore, filtration was performed twice as a further purification step (Barten et al. 2022). The collected microalgal biomass was then freeze-dried until a dry powder was obtained.

Determination of chlorophyll a, chlorophyll b, and carotenoid

Four millilitres of microalgal culture were taken and centrifuged at 3000 rpm for 10 minutes. The supernatant was discarded, and the cell pellet was washed twice with 4 ml of distilled water to remove salt residues before being centrifuged again. The cell pellet was suspended in 4 ml of absolute methanol and centrifuged for 10 minutes at 3000 rpm. The supernatant was taken to measure its absorbance using a spectrophotometer. Absorbance was measured at λ 652 nm, λ 665 nm, and λ 470 nm using methanol as the blank. Concentrations of chlorophyll a, chlorophyll b, and carotenoid pigments were calculated using formulas from Table 1 (Lichtenthaler & Buschmann 2001).

Table 1. Calculation formula for chlorophyll a, chlorophyll b, and carotenoid contents.

Component	Calculation formula
C_a (µg mL^{-1})	$16.72\ A_{665} - 9.16\ A_{652}$
C_b (µg mL^{-1})	$34.09\ A_{652} - 15.28\ A_{665}$
C_{x+c} (µg mL^{-1})	$(1000\ A_{470} - 1.63\ C_a - 104.96\ C_b)\ /221$

C_a = chlorophyll a content, C_b = chlorophyll b content, C_{x+c} = total carotenoid content

Metabolite extraction for metabolomic analysis

Fifty micrograms (50 µg) of samples, specifically A1 from the Cd-saline treatment and E3 from the control treatment, were weighed into 1.5 mL Eppendorf tubes, respectively. Each sample was soaked with 800 µL of a precooled extraction solution (methanol:water = 7:3, v/v) and 20 µL of Internal Standard 1 (IS1). The methanol-water extraction protocol was selected based on established methods for comprehensive polar metabolite recovery in UPLC-MS metabolomics studies (Salem et al. 2020; Sarkar et al. 2025). Homogenisation was performed using a weaving grinder at 50 Hz for 10 minutes, followed by water bath ultrasonication at 4 °C for 30 minutes. Subsequently, the samples were allowed to stand at −20 °C for 1 hour to enhance metabolite precipitation and extraction efficiency (Gorrochategui et al. 2021). The extracts were centrifuged at 14,000 rpm at 4 °C for 15 minutes. A volume of 600 µL of supernatant was filtered through a 0.22 µm membrane, and 20 µL of the filtered solution from each sample was combined to create a mixed quality control (QC) sample, following standard metabolomics protocols for microalgal stress studies (Liu et al. 2023).

This QC sample was used to assess the repeatability and stability of the LC/MS analysis. QC samples were injected at the beginning, middle, and end of each analytical batch, with additional QC injections every 10-15 study samples throughout the analytical sequence to monitor instrumental drift and system performance (Wang et al. 2022; Smith et al. 2023). Quality control acceptance criteria, following current metabolomics guidelines: metabolite features were required to show relative standard deviation (RSD) < 30 % for peak intensity across QC injections, RSD < 2 % for retention time, and mass accuracy < 10 ppm for reliable identification (González-Domínguez et al. 2024). Features not meeting these criteria were excluded from subsequent statistical analyses to ensure data quality and reliability. Both the filtered samples and the mixed QC samples were transferred to 1.5 mL sample vials for subsequent instrumental analysis.

UPLC-MS/MS analysis

Metabolite separation and detection were performed using a Waters UPLC I-Class Plus system coupled with a Q Exactive high-resolution tandem mass spectrometer (Thermo Fisher Scientific, USA). Each treatment group included three biological replicates (n=3) for statistical analysis. Chromatographic separation was conducted on Hypersil GOLD aQ Dim column (1.9 µm 2.1×100 mm, Thermo Fisher Scientific, USA), with mobile phase A consisting of 0.1 % formic acid in water and mobile phase B consisting of 0.1 % formic acid in acetonitrile. The column temperature was maintained at 40 °C. The gradient conditions were optimised based on established UPLC-MS metabolomics protocols (Want et al. 2012; Salem et al. 2020) and were as follows: 5 % B over 0.0-2.0 min, 5-95 % B over 2.0-22.0 min, held constant at 95 % B over 22.0-27.0 min, and washed with 95 % B over 27.1-30 min. The flow rate was 0.3 mL min^{-1}, and the injection volume was 5 µL.

Mass spectrometry conditions: Using Q Exactive (Thermo Fisher Scientific, USA), with primary and secondary mass spectrometry data acquisition following established untargeted metabolomics protocols (Gorrochategui et al. 2021; Sarkar et al. 2025). The scan range was 125–1500 m/z for positive ions and 100–1500 m/z for negative ions with a resolution of 70,000. The automatic gain control (AGC) target for MS acquisitions was set to 1×10^6 with a maximum ion injection time of 100 ms. The top three precursors were selected for subsequent MS/MS fragmentation with a maximum ion injection time of 50 ms and resolution of 30,000, and the AGC was 2×10^5. The stepped normalised collision energy was set to 20, 40, and 60 eV. ESI parameters were set as follows: Sheath gas flow rate was 40, Aux gas flow rate was 10,

positive-ion mode Spray voltage (|KV|) was 3.80, negative-ion mode Spray voltage (|KV|) was 3.20, Capillary temperature was 320 °C, Aux gas heater temperature was 350 °C.

Metabolite ion peak extraction and metabolite identification

Offline mass spectrometry data were imported into Compound Discoverer 3.3 (Thermo Fisher Scientific, USA) and analysed in combination with BMDB (BGI Metabolome Database), mzCloud, and ChemSpider online databases, generating a data matrix containing metabolite peak areas and identification results.

Metabolite identification and annotation followed the Metabolomics Standards Initiative (MSI) confidence levels to ensure reliable compound identification (Schymanski et al. 2014; Creek et al. 2024). Confidence levels were assigned as follows: Level 1 (identified metabolites) - confirmed with authentic reference standards matching exact mass, retention time, and MS/MS fragmentation patterns; Level 2 (putatively annotated compounds) - probable structures based on library spectral similarity and/or diagnostic evidence without reference standards; Level 3 (putatively characterised compound classes) - characterised to compound class level only; Level 4 (unknown compounds) - unidentified compounds with spectral or chromatographic information (Sumner et al. 2007; Blazenovic et al. 2018).

Only metabolites with MSI confidence levels 1 and 2 were included in final statistical analyses to ensure annotation reliability and reduce false positives. False discovery rate (FDR) control was applied at 5 % for multiple testing corrections during annotation scoring to maintain statistical rigor in metabolite identification (Tsugawa et al. 2015). Database matching scores were filtered using minimum spectral similarity thresholds (>70 % for mzCloud, >80 % for BMDB) and mass accuracy requirements (<5 ppm) to enhance identification confidence. The resulting data table was further analysed and processed.

Software Information: Compound Discoverer Version: v.3.3. Parameters: Parent ion mass deviation: <5 ppm; Mass deviation of fragment ions: <10 ppm; Retention time deviation: <0.2 min. Official Website: https://mycompounddiscoverer.com/

Antioxidant activity using the ABTS test

A total of 200 mg of dry microalgae samples were soaked in 15 mL of DCM:MeOH (v/v= 1:1) for 2x24 hours. Every 24 hours, the maceration solution was centrifuged at 4000 rpm for 10 minutes. The supernatant was put into a porcelain cup for evaporation to obtain the extract yield. Furthermore, the yield was weighed and dissolved in absolute methanol at a concentration of 10,000 ppm. Antioxidant was measured using ABTS reagent (2,2'-azino-bis 3-ethylbenzothiazoline-6-sulfonic acid) as follows. Samples from each treatment were prepared in concentrations of 1250, 625, 312.5, and 156.25 ppm, and subjected to antioxidant testing using the ABTS method. A total of 7.5 µL of sample was added to a 96-well microplate, followed by 142.5 µL of ABTS reagent. The mixture was homogenised and incubated for 30 min at 25 °C in darkness. Absorbance was measured at 745 nm, with each measurement performed in triplicate (Coulombier et al. 2020). Antioxidant activity was expressed as IC50 values (concentration required to inhibit 50 % of ABTS radical), calculated from dose-response curves using regression analysis. A negative control (methanol blank) was included in each assay to establish baseline absorbance. Assay validity was confirmed through positive inhibition responses across the tested concentration range, consistent with established ABTS protocols for plant extracts (reference).

Data Analysis

The experimental results of IC50, chlorophyll a (Chl_a), chlorophyll b (Chl_b), and carotenoids concentrations are expressed as means ± standard deviation (SD) of three replicates per treatment. One-way ANOVA was performed using R version 4.4.2, with significance levels tested at $p < 0.05$ (Tukey's HSD test).

The processed metabolite data and IC50 values were analysed using partial least squares (PLS) regression to assess the correlation between metabolite profiles and antioxidant activity. Data preprocessing involved normalisation of metabolite data by TIC (Total Ion Count) and imputation of missing values. PLS analysis was performed with leave-one-out (LOO) cross-validation using the plsr function in R. Regression coefficients were extracted and normalised to identify metabolites with the most significant influence on IC50 values. The statistical analysis was conducted using R version 4.4.2, and results were visualised with bar plots representing the contributions of each metabolite.

In addition, the PLS-DA model and Variable Importance in Projection (VIP) scores were constructed to evaluate the relationships between metabolites and IC50 values. These analyses were performed using MetaboAnalyst 6.0 (https://www.metaboanalyst.ca) from a dataset of 1843 metabolites obtained through UPLC-MS. For PLS-DA analysis, data preprocessing included normalisation and transformation to ensure suitability for multivariate analysis. VIP scores were calculated to identify key metabolites contributing significantly to the model's prediction. Analysis and visualisations were conducted using the MetaboAnalyst platform.

RESULTS AND DISCUSSION

Results

The experiment was designed with different treatments and growth phases, as shown in Table 2. The highest chlorophyll a and chlorophyll b contents were observed in the control treatment during the half-log phase (E1), at 18.886 mg $g^{-1}$and 16.923 mg g^{-1}, respectively. Conversely, the lowest chlorophyll a and b concentrations were found in the control treatment during the death phase (E3), namely 0.909 mg g^{-1} and 1.886 mg g^{-1}, respectively.

Total carotenoid concentrations showed variation across treatments and growth phases, with the highest level recorded in the Cd-saline treatment during the half-log phase (A1) at 1.919 mg g^{-1}. The carotenoid measurements represented the total carotenoid content, which may include various isomers such as β-carotene, lutein, zeaxanthin, and other xanthophyll derivatives that are known to have distinct antioxidant roles and stress response mechanisms in microalgae (Minhas et al. 2016; Sathasivam et al. 2019). Individual carotenoid isomer analysis would provide more detailed insights into specific stress adaptation pathways, as β-carotene primarily functions in photoprotection while lutein and zeaxanthin are involved in the xanthophyll cycle for dissipating excess light energy (Metting 1996; Lemoine & Schoefs 2010). The lowest carotenoid content was found in the control treatment during the log phase (E2) at 0.130 mg g^{-1}.

The Cd-saline treated samples demonstrated relatively lower IC50 values compared to control treatments, indicating higher antioxidant activity. The strongest antioxidant activity was observed in the Cd-saline treatment during the half-log phase (A1) with an IC50 value of 79.472 ± 3.3341 ppm (lower IC50 values indicate stronger antioxidant content). The weakest antioxidant activity was recorded in the control treatment during the log phase (E2) with an IC50 value of 387.262 ± 1.2601 ppm. Overall, the Cd-saline treatments exhibited enhanced antioxidant activity and total carotenoid content compared to control treatments, while chlorophyll levels (both a and b) were notably higher in the control treatment during the half-log phase (E1).

Table 2. Chlorophyll a, chlorophyll b, carotenoid content, and ABTS radical scavenging activities (IC50) in extracts of *C. vulgaris* under Cd-saline treatments at different growth phases.

Treatment	Sample code	IC50 (ppm)	Chl_a (µg mL^{-1})	Chl_b (µg mL^{-1})	Carotenoids (µg mL^{-1})
Cd-saline, half-log phase	A1	79.472^{d} ± 3.3341	18.494^{b} ± 0.036	14.681^{b} ± 0.018	1.919^{a} ± 0.015
Cd-saline, log phase	A2	81.820^{d} ± 3.1634	4.300^{d} ± 0.003	3.752^{d} ± 0.001	0.625^{b} ± 0.001
Cd-saline, death phase	A3	195.352^{b} ± 4.2488	1.117^{e} ± 0.011	2.959^{e} ± 0.007	0.166^{d} ± 0.002
Control, half-log phase	E1	164.985^{c} ± 2.1452	18.886^{a} ± 0.078	16.923^{a} ± 0.009	0.649^{b} ± 0.006
Control, log phase	E2	387.262^{a} ± 1.2601	6.739^{c} ± 0.005	9.483^{c} ± 0.005	0.130^{e} ± 0.003
Control, death phase	E3	79.965^{d} ± 7.8958	0.909^{f} ± 0.001	1.886^{f} ± 0.010	0.313^{c} ± 0.024

Note: Values are presented as mean ± standard deviation (n = 3). Different superscript letters within the same column indicate significant differences according to one-way ANOVA followed by Tukey's HSD (Honestly Significant Difference) test at $p < 0.05$. P-values were adjusted for multiple comparisons using the Tukey HSD procedure, which controls the family-wise error rate across all pairwise comparisons within each measured parameter (Abdi & Williams 2010).

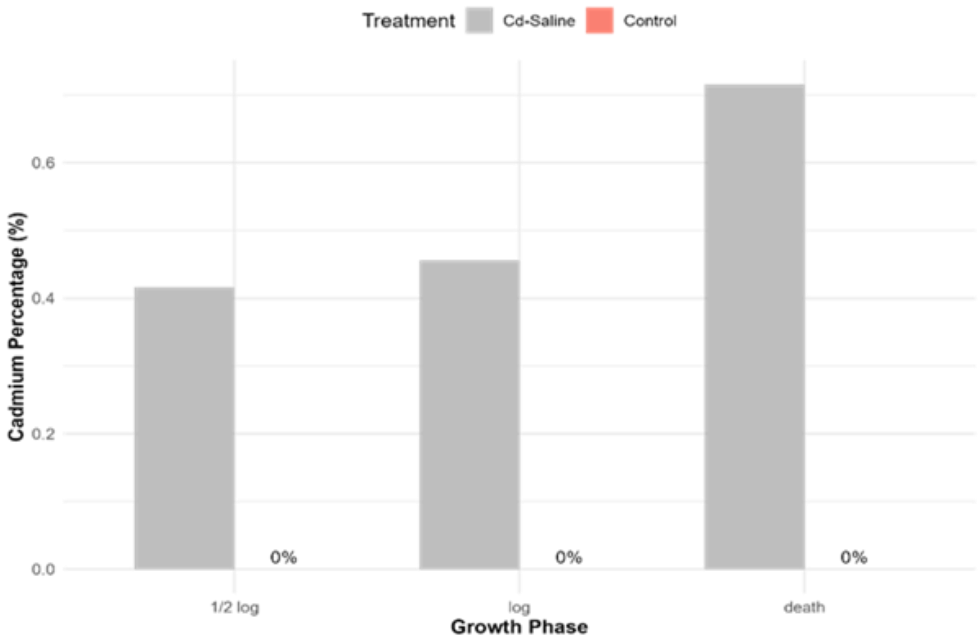

Figure 1. Cadmium accumulation percentages across different growth phases in *Chlorella vulgaris* under Control and Cd-saline treatments.

The cadmium accumulation percentages are visualised in Figure 1. The study demonstrated a clear trend in cadmium accumulation, highlighting distinct differences between the control and Cd-saline treatments across all growth phases. The control treatment consistently maintained 0 % cadmium accumulation. In contrast, the Cd-saline treatment showed a progressive increase in cadmium concentration, starting at 0.4165 % during the half-log phase, rising to 0.4560 % in the log phase, and reaching a peak of 0.7154 % in the death phase. Figure 2 presents a heatmap illustrating the correlations between cadmium percentage, pigment content, and IC50 values. Correlation

analyses revealed several significant relationships. Notably, a strong negative correlation was observed between IC50 values and chlorophyll content, indicating that samples with higher chlorophyll levels exhibited enhanced antioxidant activity, particularly during the half-log phase (E1).

Furthermore, a strong positive correlation was identified between cadmium accumulation and pigment content (chlorophyll and carotenoids), suggesting an adaptive response by *C. vulgaris* to cadmium stress, characterised by increased pigment production. Additionally, a very strong positive correlation was found between chlorophyll a and chlorophyll b levels, reflecting synchronised changes in these pigments across all treatments. This coordinated response underscores the close metabolic relationship between these chlorophyll types.

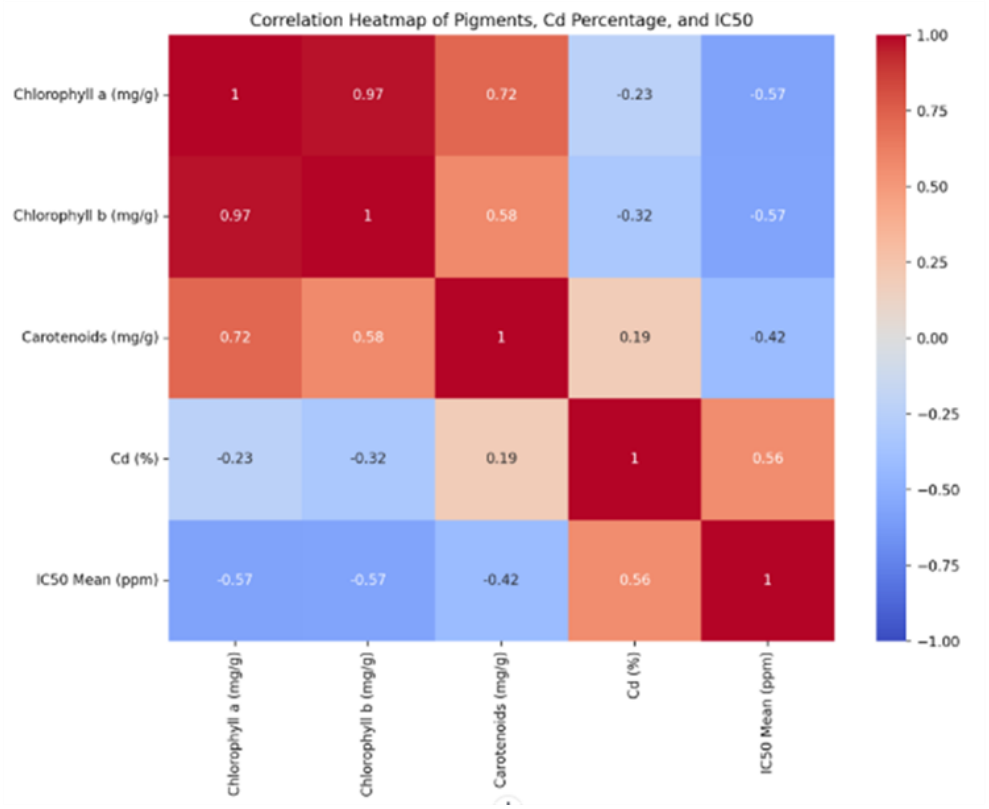

Figure 2. Heatmap showing the correlations between cadmium accumulation percentage, pigment content (chlorophyll a, chlorophyll b, and carotenoids), and IC50 values across different growth phases. The red color represents a strong positive correlation, indicating a direct relationship between variables, while the blue color represents a strong negative correlation, indicating an inverse relationship.

Peak lists generated from positive mode LC-MS data were analysed using MetaboAnalyst, with blank solvents and media excluded to avoid skewing the results. A total of 1843 compounds were identified across the six samples, with each compound representing a unique combination of m/z values and chromatographic peak areas. The metabolomics analysis revealed apparent differences between the Cd-saline and control treatments, as shown in the PLS-DA plot (Figure 3). Samples from the Cd-saline treatment formed distinct clusters, separating clearly from the control samples. The distinct clustering pattern indicates significant biochemical differences between the two treatments, likely driven by stress-induced metabolic changes. Components 1 and 2 explained 75.1 % and 7.1 % of the variance, respectively, demonstrating the ability of PLS-DA to effectively distinguish between treatment groups. The chemical diversity observed in the Cd-saline treatment suggests an adaptive response to cadmium stress, potentially involving metabolites associated with antioxidant activity and other stress-related pathways. These findings

highlight the significant metabolic alterations in *C. vulgaris* under cadmium and salinity stress.

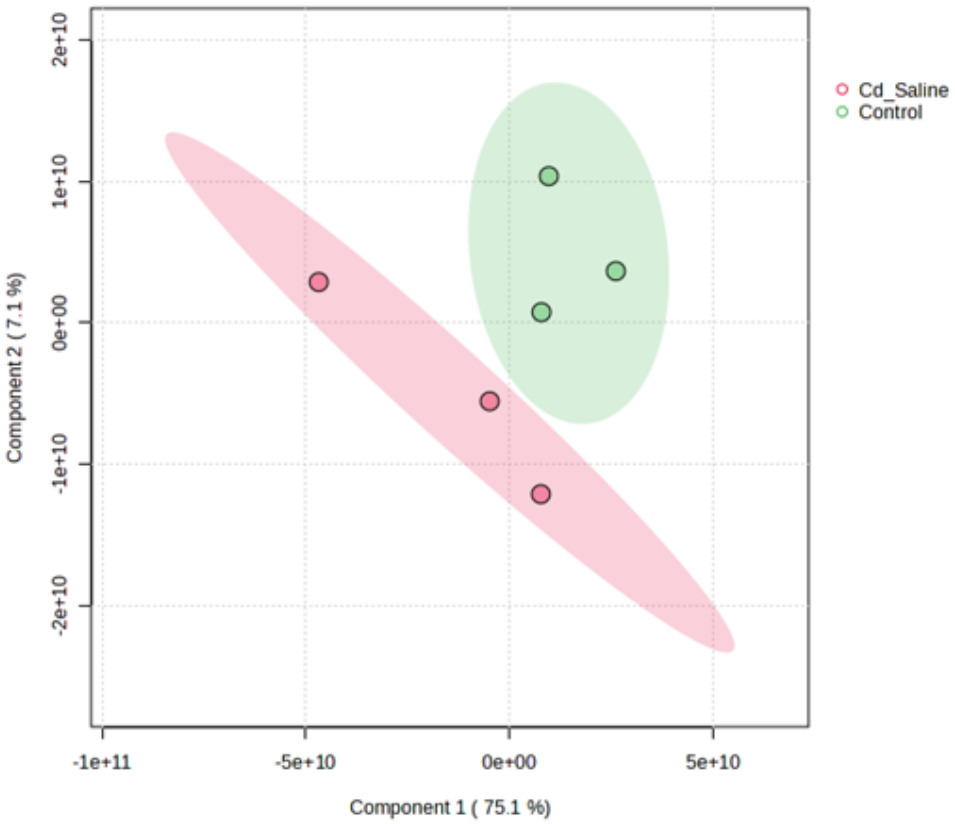

Figure 3. PLS-DA score plot illustrating the separation of metabolic profiles between Cd-saline and Control treatment groups. The distinct clustering of samples indicates significant biochemical differences driven by stress-induced metabolic changes. Components 1 and 2 accounted for 75.1 % and 7.1 % of the variance, respectively, highlighting the effectiveness of PLS-DA in distinguishing between the treatment groups.

To identify the key metabolites driving these differences, Variable Importance in Projection (VIP) scores were calculated and ranked (Figure 4). The pronounced separation observed in the PLS-DA plot emphasises the distinct metabolic profiles of *C. vulgaris* under Cd-saline and control conditions. The clustering pattern, supported by the high VIP scores of key metabolites, highlights the significant biochemical perturbations induced by cadmium and salinity stress. Notably, compounds such as stigmatellin Y, maltose, a glycolipid (1-hexadecanoyl-3-(6'-sulfo-α-D-quinovosyl)-sn-glycerol), and an aromatic organic compound ((2-phenoxy-3-pyridinyl)[3-(2-thienyl)-1H-pyrazol-1-yl]methanone) exhibited VIP (Variable Importance in Projection) scores exceeding 15. Although a threshold of VIP > 1.0 is commonly used to indicate biological relevance in PLS-DA models, exceptionally high values, such as those observed in this study, can occur due to strong discriminatory power between groups, substantial differences in metabolite abundance, or model scaling effects (Westerhuis et al. 2008; Chong et al. 2019). These elevated VIP scores emphasise the key role of these metabolites in distinguishing the metabolic response of Chlorella vulgaris under Cd-saline stress compared to control conditions. Stigmatellin Y and glycolipids were more abundant in the control group, while maltose and the aromatic organic compound ((2-phenoxy -3-pyridinyl)[3-(2-thienyl)- 1H-pyrazol-1-yl]methanone) showed higher levels under Cd-saline treatment (VIP > 15).

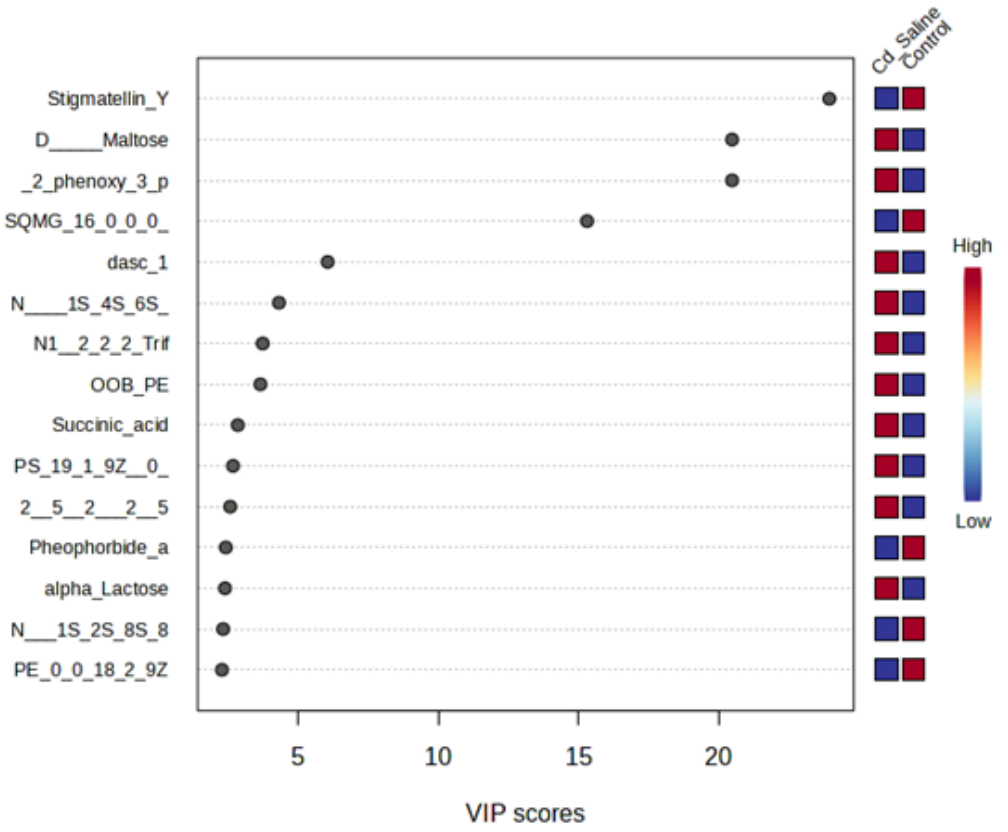

Figure 4. VIP scores of top metabolites identified through PLS-DA analysis ranked from highest to lowest. The heatmap on the right displays the relative concentrations of each metabolite in the Cd-saline and Control groups, with red indicating higher concentrations and blue indicating lower concentrations.

A Partial Least Squares (PLS) model was developed to analyse the relationship between UPLC-MS peak area data for each treatment and the biological activity assay results, represented by IC_{50} values (Pirouz 2006). The PLS model, constructed from spectral (UPLC-MS) data and antioxidant activity tests, explained a cumulative 57.93 % of variance in antioxidant activity, with LV-1 and LV-2 contributing 22.83 % and 35.10 %, respectively. The negative U PLS scores (factor-1) on the x-y relationship plot indicate a substantial contribution of individual samples to antioxidant activity. The weighted regression coefficients of metabolites in the PLS model are presented in Figure 5, illustrating their relative contributions to antioxidant activity. The loading plot provides insights into the metabolites that contribute most significantly to antioxidant activity. Table 3 lists the metabolites with significant contributions based on normalised regression coefficient values.

The most substantial negative peaks in the model were associated with pheophorbide a and 3-oxo-nonadecanoic acid, which had regression coefficient values of -14.6047 and -13.9555, respectively. These metabolites are predicted to play crucial roles in antioxidant activity, as evidenced by their direction and extreme positions on the loading plot. Significant negative regression coefficient values suggest metabolites with a major impact on biological activity. Among them, *pheophorbide a*, with the most negative regression coefficient (−14.6047), showed the highest contribution to antioxidant activity. Although pheophorbide a is a well-known chlorophyll degradation product, it has been reported to retain strong antioxidant potential due to its ability to quench singlet oxygen and scavenge free radicals (M. Saide et al. 2020). Similarly, metabolites such as 3-oxo-nonadecanoic acid and PG(16:1(9Z)/0:0) significantly contributed to biological activity, potentially through their involvement in lipid metabolism and antioxidant defence pathways. These findings support

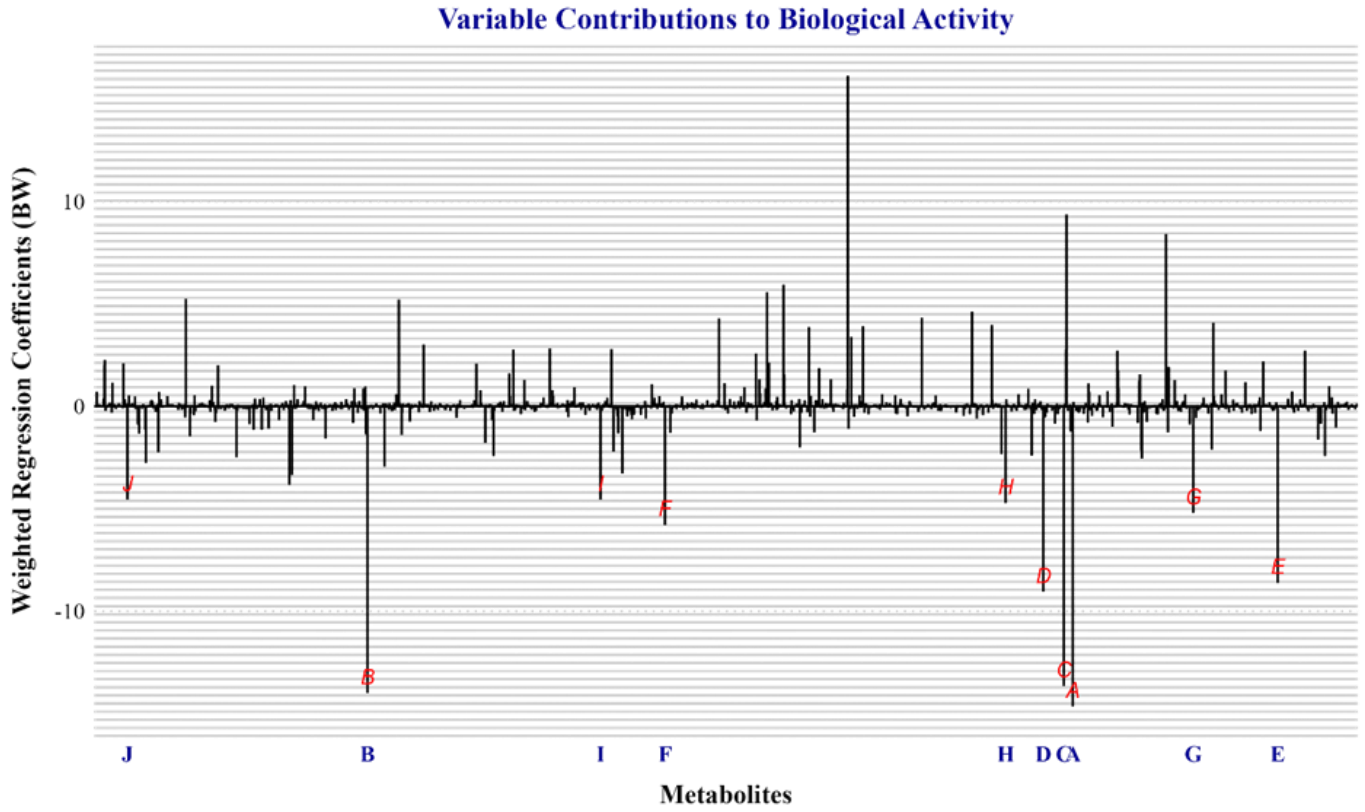

Figure 5. Weighted regression coefficients of metabolites in the PLS model correlating UPLC-MS data with antioxidant activity (IC50 Values).

Table 3. The compounds identified in the methanol extracts of *C. vulgaris* using UPLC-MS/MS contributed to the antioxidant activity.

Metabolites	Label	Database	Classification	RT (Min)	CalcMz	Formula	BW
Pheophorbide a	A	KEGG	Chlorophyll derivative	20.146	593.2755	$C_{35}H_{36}N_4O_5$	-14.6047
3-oxo-nonadecanoic acid	B	Lipidmaps	Fatty acid	13.884	313.27377	$C_{19}H_{36}O_3$	-13.9555
PG(16:1(9Z)/0:0)	C	Lipidmaps	Phospholipid	13.783	481.25784	$C_{22}H_{43}O_9P$	-13.5928
PE(19:1(9Z)/0:0)	D	Lipidmaps	Phospholipid	15.863	494.32456	$C_{24}H_{48}NO_7P$	-9.00797
Erucamide	E	mzCloud	Lipid amide	23.826	338.34156	$C_{22}H_{43}NO$	-8.57737
Elatine	F	KEGG	Terpenoid alkaloid	12.655	693.33942	$C_{38}H_{50}N_2O_{10}$	-5.74801
Stigmatellin Y	G	KEGG	Aromatic polyketide	14.118	483.27328	$C_{29}H_{40}O_6$	-5.15258
OOB-PE	H	lipid maps	Phosphatidylethanolamine derivative	15.271	562.31698	$C_{27}H_{50}NO_9P$	-4.66956
D-(+)-Maltose	I	KEGG	Disaccharide	0.873	365.10519	$C_{12}H_{22}O_{11}$	-4.51065
(2-phenoxy-3-pyridinyl)[3-(2-thienyl)-1H-pyrazol-1-yl] methanone	J	mzCloud	-	0.861	365,1053	$C_{19}H_{13}N_3O_2S$	-4.51065

the notion that more negative regression coefficient values indicate greater influence on bioactivity, consistent with the principle that lower IC_{50} values correspond to higher antioxidant capacity. Overall, the results highlight the dynamic metabolic adjustments of *Chlorella vulgaris* under stress conditions and underscore the role of specific metabolites in enhancing antioxidant potential.

Discussion

Temporal Dynamics of Antioxidant Response and Metabolic Flexibility

The antioxidant response of *C. vulgaris* to cadmium stress demonstrates a temporally coordinated cellular adaptation mechanism, with the strongest antioxidant activity (IC_{50} = 79.472 ± 3.3341 ppm, where lower IC_{50} values indicate higher antioxidant activity) observed during the half-log phase. This enhanced response during the exponential growth phase reflects the organism's metabolic flexibility, as cells in this phase possess maximum biosynthetic capacity and energy availability to rapidly deploy defensive mechanisms (Zhang et al. 2023). The heightened metabolic activity during exponential growth provides the necessary ATP and reducing equivalents to synthesise antioxidant compounds and activate enzymatic defence systems, including superoxide dismutase (SOD), catalase (CAT), and glutathione peroxidase (GPX) (Jun et al. 2003; Hameed et al. 2011).

Notably, our findings contrast with Cheng et al. (2016), who reported delayed antioxidant responses under similar cadmium exposure conditions. This discrepancy likely reflects strain-specific variations in stress response kinetics and metabolic capacity, as demonstrated by Bacova et al. (2019), who observed distinct epigenetic and metabolic responses between different microalgal species under cadmium stress. While Wang et al. (2022) observed peak antioxidant activity 48-72 hours post-exposure, our results demonstrate immediate activation within the first growth phase, suggesting that our *C. vulgaris* strain possesses more rapid stress-sensing and response mechanisms. This rapid response capability may confer ecological advantages in fluctuating environmental conditions where prompt adaptation is crucial for survival.

Cadmium Accumulation in Environmental Context

The observed cadmium accumulation of 0.7154 % (Figure 1) warrants evaluation against realistic environmental levels. Xu et al. (2024) reported cadmium concentrations ranging from 0.15-2.3 % in microalgae from contaminated freshwater systems, positioning our experimental levels within environmentally relevant ranges. However, the synergistic effects of cadmium-salinity stress create conditions more severe than single-stress scenarios, potentially explaining the pronounced metabolic responses observed. The combined stress likely disrupts cellular homeostasis through multiple pathways: cadmium interferes with essential metal enzymes while salinity imposes osmotic stress, collectively overwhelming cellular defence mechanisms and necessitating comprehensive metabolic reorganisation.

Photosynthetic Pigment Dynamics and Photoprotection

The progressive decline in chlorophyll content across growth phases reflects cadmium's direct interference with photosynthetic machinery. The identification of pheophorbide a (PPBa), a chlorophyll degradation product, suggests active chlorophyll catabolism under stress conditions. Beyond indicating photosynthetic damage, PPBa accumulation may serve photoprotective functions by dissipating excess light energy and preventing photo-oxidative damage (A. Saide et al. 2020). This dual role of PPBa—as both a stress marker and protective compound—exemplifies the complex nature of stress-induced metabolic changes, where degradation products can acquire new functional roles in

cellular defence.

The strong positive correlation between pheophorbide a and antioxidant activity (compared with M. Saide et al. 2020) likely stems from its ability to scavenge reactive oxygen species (ROS) and its role in modulating light-harvesting efficiency under stress. This relationship suggests that chlorophyll degradation, rather than being merely destructive, represents a regulated process that contributes to overall cellular antioxidant capacity.

Carotenoid-Mediated Stress Response

Carotenoid analysis revealed maximum concentrations of 1.919 mg g^{-1} during the half-log phase under Cd-saline treatment, substantially higher than the 1.2 mg g^{-1} reported by Shi et al. (2020) for *C. vulgaris* under cadmium-only stress. This elevated carotenoid accumulation under combined stress conditions indicates that salinity enhances carotenoid biosynthesis, possibly through increased expression of carotenoid biosynthetic genes or enhanced precursor availability. The temporal coincidence of peak carotenoid levels with maximum antioxidant activity underscores the critical role of these pigments in early stress response, functioning as primary (ROS) scavengers and membrane stabilisers.

Metabolic Pathway Integration and Osmotic Adjustment

Maltose Accumulation and Osmotic Regulation

The accumulation of maltose under Cd-saline stress reflects a sophisticated osmotic adjustment mechanism. As a compatible solute, maltose participates in cellular osmoregulation while maintaining enzyme functionality under osmotic stress. The elevated maltose levels likely result from activation of the trehalose-6-phosphate synthase pathway, which regulates sugar signalling and carbon partitioning during stress conditions. This osmolyte accumulation strategy aligns with recent findings by Reignier et al. (2024), who demonstrated similar osmolyte-based adaptation mechanisms in cyanobacterial communities under salt stress. This pathway not only produces osmolytes but also modulates carbon flux towards stress-protective compounds, demonstrating the interconnected nature of stress response mechanisms.

Secondary Metabolite Modulation

The depletion of stigmatellin Y in stressed samples, contrasting with its abundance in controls, suggests stress-induced reprioritisation of metabolic resources. Stigmatellin Y, associated with mitochondrial electron transport and ubiquinol-cytochrome c reductase activity (von Jagow & Ohnishi 1985), requires substantial metabolic investment for its biosynthesis. Under stress conditions, metabolic resources are redirected towards immediate survival mechanisms rather than secondary metabolite production. This finding contrasts with Mendes et al. (2024), who reported maintained stigmatellin Y levels in stress-tolerant microalgal strains, suggesting that stigmatellin Y reduction may serve as a biomarker for stress susceptibility in different strains.

Aromatic Compound Induction

The increased abundance of the aromatic organic compound ((2-phenoxy-3-pyridinyl)[3-(2-thienyl)-1H-pyrazol-1-yl]methanone) under stress conditions reflects activation of detoxification pathways. The pyridine and pyrazole rings in this compound can interact with key metabolic enzymes, potentially serving antioxidant functions or facilitating xenobiotic metabolism (Nowicka 2022). This compound's accumulation represents the organism's attempt to neutralise toxic effects through enhanced detoxification capacity.

Membrane Remodelling and Lipid Metabolism

The observed reduction in glycolipid levels, particularly (2S)-1-palmitoyl-3-O

-(6-sulfo-α-D-quinovopyranosyl)-glycerol (SQMG(16:0/0:0)), indicates extensive membrane remodelling under combined stress. Glycolipids play crucial roles in membrane stability, cell recognition, and osmotic regulation. Their depletion suggests that membrane restructuring prioritises basic membrane integrity over specialised functions, with increased presence of phosphatidylglycerol and phosphatidylethanolamine derivatives compensating for lost glycolipid functions.

Proposed Integrated Stress Response Model

Based on our findings, we propose a comprehensive model of metabolic pathway integration under combined Cd-salinity stress. The response begins with initial stress detection through rapid activation of ROS-scavenging systems and carotenoid biosynthesis, followed by osmotic adjustment via maltose accumulation through trehalose-6-phosphate synthase pathway activation. Simultaneously, membrane adaptation occurs through glycolipid reduction and phospholipid restructuring to maintain membrane integrity. Resource reallocation becomes evident as secondary metabolite synthesis (stigmatellin Y) decreases in favour of primary defence mechanisms, while detoxification enhancement proceeds through aromatic compound accumulation to neutralize toxic effects. Finally, photosynthetic adjustment involves controlled chlorophyll degradation with pheophorbide a accumulation for photoprotection, creating an integrated cellular response that maintains viability under combined stress conditions.

Methodological Considerations and Limitations

Several methodological limitations warrant acknowledgment. The untargeted metabolomics approach, while comprehensive, may miss low-abundance stress-responsive metabolites such as proline, which is commonly induced under abiotic stress but was not detected in our analysis. This absence likely reflects either concentrations below detection limits or matrix effects during LC-MS/MS analysis. Additionally, ionisation efficiency variations and matrix effects in LC-MS/MS analysis may lead to underestimation of certain metabolite classes.

The batch culture system employed may introduce temporal variations in nutrient availability and waste accumulation, potentially confounding metabolic responses attributed solely to cadmium-salinity stress. Future investigations would benefit from continuous culture systems and integration of multiple analytical platforms (NMR, GC-MS, targeted metabolomics) to achieve more complete metabolic profiling.

Environmental and Biotechnological Implications

The demonstrated cadmium accumulation capacity (0.7154 %) within environmentally relevant ranges, coupled with maintained antioxidant activity, positions *C. vulgaris* as a promising candidate for bioremediation applications. The strain's ability to rapidly activate defensive mechanisms while accumulating significant metal concentrations suggests potential for dual-purpose systems combining wastewater treatment with valuable biomass production.

The temporal specificity of antioxidant responses highlights the importance of harvest timing for maximising bioactive compound yields. The half-og phase emergence as the optimal harvest point for antioxidant activity provides practical guidance for industrial cultivation protocols.

CONCLUSIONS

This study successfully investigated the effects of combined cadmium-salinity stress on *C. vulgaris* InaCCM49, revealing significant enhancements in antioxidant capacity (IC_{50} = 79.472 ppm, 51.8% improvement over controls) and

carotenoid content (1.919 mg g^{-1}) during the half-log phase. UPLC-MS/MS coupled with PLS analysis identified key metabolites contributing to antioxidant activity, with pheophorbide a and 3-oxo-nonadecanoic acid showing the strongest correlations (regression coefficients of -14.6047 and -13.9555, respectively). Metabolomic profiling revealed distinct stress-responsive metabolites: maltose and phenolic derivatives accumulated under stress, while stigmatellin Y and glycolipids were depleted, indicating metabolic resource reallocation toward primary defence mechanisms. These findings demonstrate strain-specific metabolic adaptations of *C. vulgaris* InaCCM49 under combined stress, providing insights for optimizing algal cultivation in polluted environments and strategic harvest timing to maximize bioactive compound yields.

AUTHOR CONTRIBUTION

D.E. designed the research, collected and the data, and wrote the manuscript. R.S.R. analysed the data and wrote the manuscript. A.E.R. collected and analysed the data. H.P. and N. supervised the entire process.

ACKNOWLEDGMENTS

The research team would like to thank Prof. Adi Setyo Purnomo, Ph.D., who provided a centrifuge and a freeze dryer in the Microorganism Chemistry Laboratory, Department of Chemistry, ITS Surabaya.

CONFLICT OF INTEREST

The authors declare no conflict of interest regarding funding, the research process, or the writing of this article.

REFERENCES

Abdi, H. & Williams, L.J., 2010. Tukey's honestly significant difference (HSD) test. *Encyclopedia of Research Design*, 1, pp.1–5.

Atabayeva, S.D. et al., 2022. Rice Plants (*Oryza sativa* L.) under Cd Stress in Fe Deficiency Conditions. *BioMed Research International*, 2022(1), 7425085 . doi: 10.1155/2022/7425085.

Bacova, R. et al., 2019. The effects of 5 azacytidine and cadmium on global 5 methylcytosine content and secondary metabolites in the freshwater microalgae *Chlamydomonas reinhardtii* and *Scenedesmus quadricauda*. *Journal of Phycology*, 55, pp.329–342. doi: 10.1111/jpy.12824

Barten, R. et al., 2022. Expanding the upper-temperature boundary for the microalga *Picochlorum* sp. (BPE23) by adaptive laboratory evolution. *Biotechnology Journal*, 17, 2100659. doi: 10.1002/biot.202100659

Blazenovic, I. et al., 2018. Comprehensive comparison of annotation strategies for untargeted metabolomics. *Analytical Chemistry*, 90(12), pp.732–742. doi: 10.1021/acs.analchem.8b00800

Chen, J. et al., 2020. Hydrothermal Carbonization of Microalgae-Fungal Pellets: Removal of Nutrients from the Aqueous Phase Fungi and Microalgae Cultivation. *ACS Sustainable Chemistry & Engineering*, 8(45), pp.16823–16832. doi: 10.1021/acssuschemeng.0c05441

Cheng, J. et al., 2016. The effect of cadmium on the growth and antioxidant response for freshwater algae *Chlorella vulgaris*. *SpringerPlus*, 5, 1290. doi: 10.1186/s40064-016-2961-4

Chia, M.A. et al., 2013. Effects of cadmium and nitrogen on lipid composition of *Chlorella vulgaris* (Trebouxiophyceae, Chlorophyta). *European Journal of Phycology*, 48(1), pp.1–11. doi: 10.1080/09670262.2012.750687

Chong, J., Wishart, D.S. & Xia, J., 2019. Using MetaboAnalyst 4.0 for Comprehensive and Integrative Metabolomics Data Analysis. *Current Protocols in Bioinformatics*, 68(1), e86. doi: 10.1002/cpbi.86

Coronado-Reyes, J.A. et al., 2022. *Chlorella vulgaris*, a microalgae important to be used in Biotechnology: a review. *Food Science and Technology*, 42, e37320. doi: 10.1590/fst.37320

Coulombier, N. et al., 2020. Impact of Light Intensity on Antioxidant Activity of Tropical Microalgae. *Marine Drugs*, 18(2), 122. doi: 10.3390/md18020122

Creek, D.J. et al., 2024. Best practices and confidence levels in metabolite annotation. *Metabolites*, 14(1), 11. doi: 10.3390/metabo14010011

El-fayoumy, E.A. et al., 2021. Evaluation of antioxidant and anticancer activity of crude extract and different fractions of *Chlorella vulgaris* axenic culture grown under various concentrations of copper ions. *BMC Complementary Medicine and Therapies*, 21(1), 51. doi: 10.1186/s12906-020-03194-x

González-Domínguez, Á. et al., 2024. QC*omics*: Recommendations and Guidelines for Robust, Easily Implementable and Reportable Quality Control of Metabolomics Data. *Analytical Chemistry*, 96(3), pp.1064–1072. doi: 10.1021/acs.analchem.3c03660

Gonzalez-Esquer, C.R. et al., 2019. Demonstration of the potential of *Picochlorum soloecismus* as a microalgal platform for the production of renewable fuels. *Algal Research*, 43, 101658. doi: 10.1016/j.algal.2019.101658

Gorrochategui, E. et al., 2021. Recent advances in high-resolution mass spectrometry for environmental metabolomics. *Environmental Science & Technology*, 55(7), pp.4139–4152. doi: 10.1021/acs.est.0c07979

Hameed, A. et al., 2011. Differential activation of the enzymatic antioxidant system of *Abelmoschus esculentus* L. under $CdCl_2$ and $HgCl_2$ exposure. *Brazilian Journal of Plant Physiology*, 23(1), pp.46–54. doi: 10.1590/S1677-04202011000100007

Hawrył, A. et al., 2020. HPLC Fingerprint Analysis with the Antioxidant and Cytotoxic Activities of Selected Lichens Combined with the Chemometric Calculations. *Molecules*, 25(18), 4301. doi: 10.3390/molecules25184301

Hiremath, S. & Mathad, P., 2022. Secondary Metabolites of *Chlorella Vulgaris* Under Saline Stress. *International Journal of Scientific Research in Science and Technology*, pp.424–429. doi: 10.32628/IJSRST229650

Jun, M. et al., 2003. Comparison of Antioxidant Activities of Isoflavones from Kudzu Root (*Pueraria lobata* Ohwi). *Journal of Food Science*, 68(6), pp.2117–2122. doi: 10.1111/j.1365-2621.2003.tb07029.x

Lemoine, Y. & Schoefs, B., 2010. Secondary ketocarotenoid astaxanthin biosynthesis in algae: a multifunctional response to stress. *Photosynthesis Research*, 106(1–2), pp.155–177. doi: 10.1007/s11120-010-9573-2

Lichtenthaler, H.K. & Buschmann, C., 2001. Chlorophylls and Carotenoids: Measurement and Characterization by UV-VIS Spectroscopy. *Current Protocols in Food Analytical Chemistry*, 1(1), pp.F4.3.1-F4.3.8. doi: 10.1002/0471142913.faf0403s01

Liu, Y. et al., 2021. Biofuels for a sustainable future. *Cell*, 184(6), pp.1636–1647. doi: 10.1016/j.cell.2021.01.052

Mendes, A.R. et al., 2024. Chemical Compounds, Bioactivities, and Applications of *Chlorella vulgaris* in Food, Feed and Medicine. *Applied Sciences*, 14(23), 10810. doi: 10.3390/app142310810

Metting, F.B., 1996. Biodiversity and application of microalgae. *Journal of Industrial Microbiology*, 17(5–6), pp.477–489. doi: 10.1007/BF01574796

Minhas, A.K. et al., 2016. A review on the assessment of stress conditions for simultaneous production of microalgal lipids and carotenoids. *Frontiers in Microbiology*, 7, 546. doi: 10.3389/fmicb.2016.00546

Nowicka, B., 2022. Heavy metal–induced stress in eukaryotic algae—mechanisms of heavy metal toxicity and tolerance with particular emphasis on oxidative stress in exposed cells and the role of antioxidant response. *Environmental Science and Pollution Research*, 29(12), pp.16860–16911. doi: 10.1007/s11356-021-18419-w

Pantami, H.A. et al., 2020. Comprehensive GCMS and LC-MS/MS Metabolite Profiling of *Chlorella vulgaris*. *Marine Drugs*, 18(7), 367. doi: 10.3390/md18070367

Pirouz, D.M., 2006. An Overview of Partial Least Squares. *SSRN Electronic Journal*, pp.1–16.

Reignier, O. et al., 2024. Effects of salinity and nutrient stress on a toxic freshwater cyanobacterial community and its associated microbiome: An experimental study. *Environmental Microbiology Reports*, 16, e70029. doi: 10.1111/1758-2229.13029

Saide, A., Lauritano, C. & Ianora, A., 2020. Pheophorbide a: State of the Art. *Marine Drugs*, 18(5), 257. doi: 10.3390/md18050257

Saide, M., Abdullah, M. & Hossain, M.A., 2020. Pheophorbide a as a chlorophyll derivative with multifunctional biological activities: A review. *Journal of Photochemistry and Photobiology B: Biology*, 204, 111801. doi: 10.1016/j.jphotobiol.2020.111801

Salem, M.A. et al., 2020. An improved UPLC–MS-based method for untargeted metabolomics analysis of plant tissues. *Metabolomics*, 16(3), 13. doi: 10.1007/s11306-020-1654-1

Sarkar, A. et al., 2025. Untargeted metabolomics for systems biology and environmental studies: Methods and applications. *Trends in Analytical Chemistry*, in press.

Sathasivam, R. et al., 2019. Microalgae metabolic engineering to improve the energy balance for biodiesel production. *Applied Energy*, 254, 113702. doi: 10.1016/j.apenergy.2019.113702

Schymanski, E.L. et al., 2014. Identifying small molecules via high resolution mass spectrometry: Communicating confidence. *Environmental Science & Technology*, 48(4), pp.2097–2098. doi: 10.1021/es5002105

Shi, T.-Q. et al., 2020. Stresses as First-Line Tools for Enhancing Lipid and Carotenoid Production in Microalgae. *Frontiers in Bioengineering and Biotechnology*, 8, 610. doi: 10.3389/fbioe.2020.00610

Smith, J. et al., 2023. SP3-based host cell protein monitoring in AAV-based gene therapy products using LC-MS/MS. *European Journal of Pharmaceutics and Biopharmaceutics*, 189, pp.276–280. doi: 10.1016/j.ejpb.2023.06.019

Sumner, L.W. et al., 2007. Proposed minimum reporting standards for chemical analysis. *Metabolomics*, 3(3), pp.211–221. doi: 10.1007/s11306-007-0082-2

Tsugawa, H. et al., 2015. MS-DIAL: data-independent MS/MS deconvolution for comprehensive metabolome analysis. *Nature Methods*, 12(6), pp.523–526. doi: 10.1038/nmeth.3393

Umar, A.H. et al., 2021. Untargeted Metabolomics Analysis Using FTIR and UHPLC-Q-Orbitrap HRMS of Two *Curculigo* Species and Evaluation of Their Antioxidant and α-Glucosidase Inhibitory Activities. *Metabolites*, 11(1), 42. doi: 10.3390/metabo11010042

von Jagow, G. & Ohnishi, T., 1985. The chromone inhibitor stigmatellin - binding to the ubiquinol oxidation center at the C-side of the mitochondrial membrane. *FEBS Letters*, 185(2), pp.311–315. doi: 10.1016/0014-5793(85)80929-7

Walne, P.R.,1970. *Studies on the food value of nineteen genera of algae to juvenile bivalves of the genera Ostrea, Crassostrea, Mercenaria and Mytilus*, London: Her Majesty's Stationery Office.

Wang, J. et al., 2022. Application of Microalgal Stress Responses in Industrial Microalgal Production Systems. *Marine Drugs*, 20(1), 30. doi: 10.3390/md20010030

Want, E.J. et al., 2012. Global metabolic profiling of animal and human tissues via UPLC–MS. *Nature Protocols*, 7(5), pp.813–838. doi: 10.1038/nprot.2012.024

Westerhuis, J. et al., 2008. Assessment of PLSDA cross validation. *Metabolomics*, 4, pp.81–89. doi: 10.1007/s11306-007-0099-6

Xu, P. et al., 2024. Cadmium-Induced Physiological Responses, Biosorption and Bioaccumulation in *Scenedesmus obliquus*. *Toxics*, 12(4), 262. doi: 10.3390/toxics12040262

Zhang, L. et al., 2023. The differential modulation of secondary metabolism induced by a protein hydrolysate and a seaweed extract in tomato plants under salinity. *Frontiers in Plant Science*, 13, 1072782. doi: 10.3389/fpls.2022.1072782